found extensive applications in data processing for least-square approximations.[3] In closing it should be noted that Eq. (9) can be obtained by invoking the Orthogonal Projection Lemma,[4] thus providing a geometric interpretation to the optimal features of Eq. (10).

Case B: $n<m$

Again, with no loss of generality, it can be assumed that A is of full rank, i.e.,

$$\text{rank}\,(A)=n \tag{11}$$

If, however, rank$(A)<n$, it implies that some of the equations are merely a linear combination of the others and therefore may be deleted without loss of information, thereby reducing the case rank$(A)<n$ to the case rank$(A)=n$. Moreover, if A is a square singular matrix, it can be reduced to case B after proper deletion of the dependent rows of A.

As posed, Eqs. (1) and (11) with $n<m$ yield an infinite number of solutions, the "optimal" of which is the one having the smallest norm. Therefore, one is confronted with a constrained minimization problem, where the minimization of $\|x\|$ (or equivalently $(1/2)\|x\|^2$) is to be accomplished subject to Eq. (1). Adjoining the constraint, via a vector of Lagrange Multipliers (λ), to the fundamental to be minimized we obtain

$$H=\tfrac{1}{2}\|x\|^2+\lambda^T(y-Ax)=\tfrac{1}{2}x^Tx+\lambda^T(y-Ax) \tag{12}$$

Evaluating the respective gradients

$$\partial H/\partial x=x-A^T\lambda=0 \tag{13}$$

$$\partial H/\partial\lambda=y-Ax=0 \tag{14}$$

From Eq. (13)

$$x=A^T\lambda \tag{15}$$

Substitution of Eq. (15) in Eq. (14) yields

$$y=AA^T\lambda \tag{16}$$

or

$$\lambda=(AA^T)^{-1}y \tag{17}$$

The existence of $(AA^T)^{-1}$ is guaranteed by virtue of Eq. (11). Substitution of Eq. (17) in Eq. (15) yields

$$x=A^T(AA^T)^{-1}y \tag{18}$$

In this case ($n<m$) the generalized inverse of A is given by

$$A^+=A^T(AA^T)^{-1} \tag{19}$$

For the sake of completeness it should be noted that the norm minimization of $\|e\|$ and $\|x\|$ of Eqs. (6) and (12), respectively, can be performed relative to extended vector norms, where a norm of a vector w is defined as w^TQw and Q is a compatible positive definite weighting matrix. By so doing, one can choose the relative emphasis of the magnitudes of the vector components being minimized.

For case A, Eq. (6) becomes

$$z=e^TQe=(y-Ax)^TQ(y-Ax) \tag{20}$$

with the solution

$$x=(A^TQA)^{-1}A^TQy \tag{21}$$

For case B, Eq. (12) becomes

$$H=\tfrac{1}{2}x^TQx+\lambda^T(y-Ax) \tag{22}$$

with the solution

$$x=Q^{-1}A^T(AQ^{-1}A^T)^{-1} \tag{23}$$

A unified framework has been presented showing that the generalized inverse of a matrix can be viewed as a result of a minimization problem leading to a practical engineering interpretation.

References

[1] Penrose, R., "A Generalized Inverse for Matrices," *Proceedings of the Cambridge Philosophical Society*, Vol. 51, 1955, pp. 406-413.

[2] Hassig, H. J., "Practical Aspect of the Generalized Inverse of a Matrix," *AIAA Journal*, Vol. 13, Nov. 1975, pp. 1530-1531.

[3] Sorenson, H. W., "Kalman Filtering Techniques," *Advances in Control Systems*, edited by C. T. Leondes, 1966, pp. 219-340.

[4] Luenberger, D. G., *Optimization by Vector Space Methods*, Wiley, New York, 1969.

Resizing Procedure for Structures Under Combined Mechanical and Thermal Loading

Howard M. Adelman*
NASA Langley Research Center, Hampton, Va.
and
R. Narayanaswami†
Old Dominion University Norfolk, Va.

Introduction

PROBABLY the most widely used approach for sizing of flight structures under strength and minimum gage constraints is fully-stressed design (FSD). In this method the structural sizes are iterated with the step size depending on the ratio of the total stress to the allowable stress.[1-3] The FSD procedure traditionally is used to obtain, at a reasonable computational cost, designs which, if not at a minimum weight, are at least acceptably close to the minumum weight.[2]

Almost all of the experience with FSD has been with structures primarily under mechanical loading as opposed to thermal loading. The temptation in including thermal loads in FSD is simply to continue to use the total stresses in computing the iteration step size. This approach seems satisfactory when mechanical stresses dominate the thermal stresses.[4] Convergence may be slow, however, when thermal stresses are comparable to mechanical stresses. The slowed convergence is associated with relative insensitivity of the thermal stresses to changes in structural sizing. Therefore, procedures are needed which take into account the differing responses of thermal and mechanical stresses to changes in structural sizes.

An improved variant of FSD for uniaxial stress members was described in Ref. 4 and demonstrated for automated sizing of truss-type structures. For problems having sub-

Received Feb. 13, 1976; revision received June 3, 1976.
Index categories: Structural Design, Optimal; Thermal Stresses.

*Research Engineer, Thermal Structures Branch, Structures and Dynamics Div.
†Research Associate Professor of Mechanical Engineering and Mechanics.

stantial thermal stress, the new procedure (called thermal fully-stressed design or TFSD was found to converge in far fewer iterations than ordinary FSD. This Note shows an extension of the TFSD procedure to biaxial stress members using a Von Mises Failure criterion. The TFSD resizing procedure for uniaxial stress members is restated, the new procedure for biaxial stress members is developed, and results are given from an application of the two procedures to size a simplified wing structure.

TFSD Algorithm for Uniaxial Stress Members

The TFSD resizing algorithm for uniaxial stress members (rods) is[4]

$$A_{i+1} = \frac{\sigma_{Mi}}{(\sigma_{a,M} - \sigma_{Ti})} A_i \tag{1}$$

where i is the iteration number. In Eq. (1) σ_M is the stress caused by mechanical loads acting alone, σ_T is the stress caused by thermal loads acting alone, and $\sigma_{a,M}$ is either the tensile or compressive allowable stress, depending on the sign of σ_M. The algorithm of Eq. (1) drives each element toward the condition

$$\sigma_M/(\sigma_{a,M} - \sigma_T) = 1 \tag{2}$$

Thus, the mechanical stress is driven toward an effective allowable stress given by the algebraic difference between the thermal stress and material allowable stress. For later reference, the usual FSD algorithm is given by

$$A_{i+1} = [(\sigma_{Mi} + \sigma_{Ti})/\sigma_a]\ A_i \tag{3}$$

where σ_a is either the tensile or compressive allowable stress, depending on the sign of the total stress as given by the numerator. The algorithm is Eq. (3) drives each element toward the condition $(\sigma_M + \sigma_T)/\sigma_a = 1$.

Development of TFSD Resizing Algorithm for Biaxial Stress Members

The Von Mises failure criterion for isotropic materials subject to a general state of plane stress is

$$V(\sigma_x, \sigma_y, \sigma_{xy}) = [\sigma_x^2 + \sigma_y^2 - \sigma_x\sigma_y + 3\sigma_{xy}^2]^{1/2} = \sigma_a \tag{4}$$

where σ_x and σ_y are normal stresses along orthogonal coordinate directions in the plane of the element; σ_{xy} is the shear stress on that plane; and σ_a is the allowable stress. In preparation for generalizing the resizing formula from uniaxial to biaxial stress members, rearrange Eq. (1) as follows

$$\frac{\sigma_{Mi}}{A_{i+1}/A_i} + \sigma_{Ti} = \sigma_{a,M} \tag{5}$$

By analogy, the corresponding statement for biaxially stressed members is

$$V\left(\frac{\sigma_{xMi}}{r_i} + \sigma_{xTi}, \frac{\sigma_{yMi}}{r_i} + \sigma_{yTi}, \frac{\sigma_{xyMi}}{r_i} + \sigma_{xyTi}\right) = \sigma_a \tag{6}$$

where $r_i = t_{i+1}/t_i$ and t is the element thickness. Expanding Eq. (6) using Eq. (4) gives

$$(V_{T,i}^2 - \sigma_a^2) r_i^2 + b_i r_i + V_{M,i}^2 = 0 \tag{7}$$

where

$$V_T^2 = \sigma_{xT}^2 + \sigma_{yT}^2 - \sigma_{xT}\sigma_{yT} + 3\sigma_{xyT}^2 \tag{8a}$$

$$V_M^2 = \sigma_{xM}^2 + \sigma_{yM}^2 - \sigma_{xM}\sigma_{yM} + 3\sigma_{xyM}^2 \tag{8b}$$

$$b = 2\sigma_{xT}\sigma_{xM} + 2\sigma_{yT}\sigma_{yM} - \sigma_{xT}\sigma_{yM} - \sigma_{yT}\sigma_{xM} + 6\sigma_{xyT}\sigma_{xyM} \tag{8c}$$

Solving Eq. (7) by the quadratic formula gives the resizing algorithm

$$t_{i+1} = \left\{ \frac{b_i}{2(\sigma_a^2 - V_{Ti}^2)} \pm \left[\frac{b_i^2}{4(\sigma_a^2 - V_{Ti}^2)^2} + \frac{V_{Mi}^2}{\sigma_a^2 - V_{Ti}^2} \right]^{1/2} \right\} t_i \tag{9}$$

The choice of sign in front of the bracketed quantity is dictated by the requirement that the quantity in braces be positive since only positive thicknesses are physically meaningful. When $V_T < \sigma_a$ the positive sign must be chosen. When $V_T > \sigma_a$ and $b > 0$ the algorithm is inapplicable since no acceptable design exists without thermal stress reduction by nonstructural means. When $V_T > \sigma_a$ and $b < 0$, either the positive or negative sign may be used provided the quantity in brackets is positive. In the latter case intuition would suggest the choice of the negative sign since the minimum weight is sought. The authors' use of the algorithm has been limited to cases wherein $V_T < \sigma_a$ and hence the positive sign was used exclusively in Eq. (9).

For later reference, the corresponding FSD resizing algorithm used to compare results with TFSD is

$$t_{i+1} = (V_i/\sigma_a)\, t_i \tag{10}$$

where V is defined Eq. (4).

The TFSD procedure has the property of FSD that every element is fully-stressed for at least one load case unless a size constraint (such as minimum gage) is active. Further, in the authors' experience, TFSD and FSD always have converged to the same design although no proof that this always will occur has been produced. Finally, it is noted that TFSD and FSD both have the property that the final designs are minimum weight for statically determinant structures.

Application to a Built-Up Wing

To illustrate the application of the TFSD resizing algorithm and to compare the algorithm with ordinary FSD, calculations were carried out using a computer program incorporating both the TFSD and FSD procedures. Finite-element methods based on standard rod elements and the "TRIM 6" triangular membrane elements[5] were used for the analyses.

The struture in the calculations is a simplified low-aspect ratio built-up wing shown in Fig. 1. The ribs and spars are modeled by trusses with a total of 85 rod elements. The upper and lower skins are each modeled by five membrane elements. As a result there are a total of 95 design variables in the problem including rod areas and membrane thicknesses. The finite-element model has 36 grid points. Details of the finite-element model have been omitted and the loads and temperatures are not included in this Note but are available in Ref. 6.

Using the TFSD procedure [Eqs. (1) and (9)] and the FSD procedure [Eqs. (3) and (10)], designs were obtained for each of four separate load cases all having the same mechanical loads but having different levels of temperatures applied. The final designs for the four cases are detailed in Ref. 6, however, some of the salient characteristics of the final designs are mentioned herein. The TFSD and FSD designs were found to be identical as was expected. Of the 85 bars, 21 are fully-stressed and 64 are at a minimum gage. Also, of the 10 membranes, 7 are fully-stressed and 3 are sized at minimum gage. Generally, the fully-stressed bars are those oriented in the yz plane to carry the spanwise bending loads. If minimum gage constraints had not been specified, the structure would be essentially a series of trusses in the yz plane joined by a small number of bars along the leading edge of the wing and covered with the membranes. This structure would be nearly statically determinate and reflects the tendency of fully-stressed design procedures to drive structures to static determinancy when a

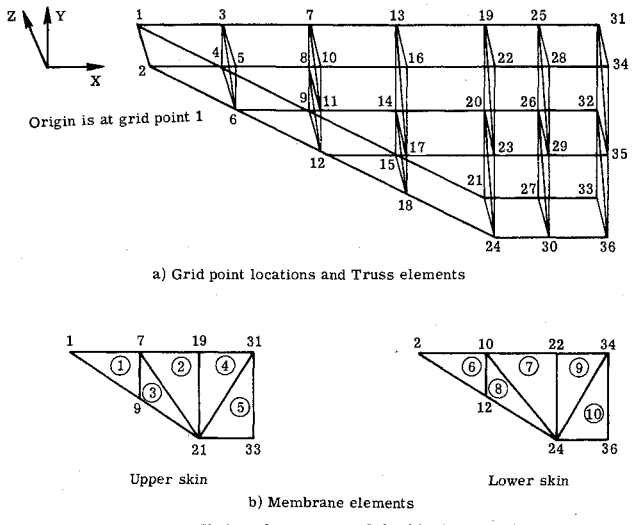

Fig. 1 Finite-element model of built-up wing.

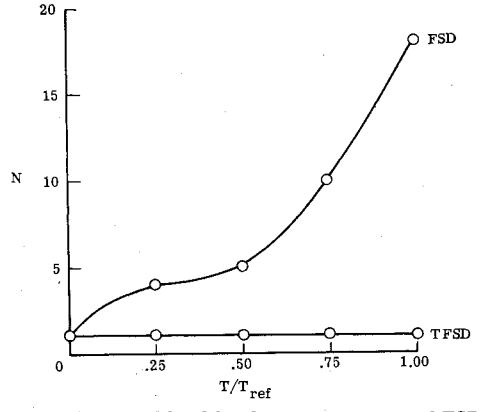

Fig. 2 Effect of thermal load level on convergence of FSD as compared to TFSD for sample problem. N = number of iterations for convergence within 5% of final mass.

single load case is applied and only strength constraints are enforced.[4] The largest proportion of the structural weight (80%) is represented in the membranes (skin). The thickest portions of the skin are represented by elements 4 and 5 in the upper skin and elements 9 and 10 in the lower skin as these are the regions of highest loading. Although the present procedure is based on sizing for strength and not deflections, the deflections of the final designs were within reasonable bounds. The maximum deflection occurred in the Z direction at grid point 33 and was about 5% of the wing semispan.

The significant result of these calculations from the standpoint of the efficiency of the TFSD algorithm is the relative number of iterations required by FSD and TFSD to converge from an initial trial design to within some arbitrary percentage (in this work 5%) of the final mass. TFSD achieved this degree of convergence in a single iteration for all four cases. The required number of iterations for FSD (N_{FSD}) is given in Table 1 and plotted in Fig. 2 against T/T_{ref} where T_{ref} represents the highest level of thermal loading. As expected, the performance of TFSD relative to FSD shows a strong increase as thermal loads measured by T/T_{ref} become larger.

Table 1 Effect of temperature on relative efficiency of FSD and TFSD for sample problem

Iterations	T/T_{ref}				
	0.	0.25	0.50	0.75	1.0
N_{FSD}	1	4	5	10	18
N_{TFSD}	1	1	1	1	1

For this example as well as for the examples of Ref. 4, thermal stresses are quite insensitive to structural sizing. The superiority of TSFD for these examples is associated with this insensitivity. This will be clear if we imagine a case where thermal stresses are completely independent of structural size is which case TSFD obviously would be superior. It seems reasonable that a broad range of structures will exhibit the relative insensitivity of thermal stresses to sizing. Consequently, the TSFD procedure should be widely useful for structures under combined thermal and mechanical loads.

References

[1] Giles, G. L. Blackburn, C.L., and Dixon, S.C., "Automated Procedures for Sizing Aerospace Vehicle Structures (SAVES)," *Journal of Aircraft*, Vol. 9, Dec. 1972, pp. 812-819.

[2] Lansing, W., Dwyer, W., Emerton, R., and Renalli, E., "Application of Fully-Stressed Design Procedures to Wing and Empennage Structures," *Journal of Aircraft*, Vol. 8, Sept. 1971, pp. 683-688.

[3] Gellatly, R.A., Gallagher, R.H., and Luberacki, W.A., "Development of a Procedure for Automated Synthesis of Minimum Weight Structures," FDL-TDR-64-141, Oct. 1964, U.S. Air Force; available from DDC as AD 611 310.

[4] Adelman, H.M., Walsh, J.L., and Narayanaswami, R. "An Improved Method for Optimum Design of Mechanically and Thermally Loaded Structures," NASA TN D-7965, 1975.

[5] Argyris, J.H., "Triangular Elements with Linearly Varying Strain for the Matrix Displacement Method," *Journal of Royal Aeronautical Society*, Vol. 69, Oct. 1965, pp. 711-713.

[6] Adelman, H.M. and Naraynaswami, R., "Resizing Procedure for Optimum Design of Structures Under Combined Mechanical and Thermal Loading," NASA TM X-72816, Jan. 1976.

Stagnation Region Heat Transfer in Hypersonic Particle Environments

Duane T. Hove*
Science Applications, Inc., El Segundo, Calif.

and

Edward Taylor†
Space and Missile Systems Organization, El Segundo, Calif.

Introduction

BLUNT bodies subjected to particle laden hypersonic flows can experience a stagnation region convective heat transfer significantly greater than in clear air. This phenomenon first was observed in an erosion wind tunnel when a titanium model ignited and burned even though flow conditions were thought to be insufficient to raise the model to the ignition temperature.[1] Subsequent test programs in two hypersonic wind tunnels provided further evidence of augmented heating in particle laden flows and indicated that heating rates are insensitive to model shape and size.[2,3] Dunbar, et. al., correlated the available heat-transfer data in terms of Stanton number as a function of the dust and debris/air mass flux ratio[3] but offered no phenomenological explanation for the success of this method. In order to interpret test results and to extrapolate confidently low Mach number, low Reynolds number ground test data[2,3] to reentry con-

Received Feb. 17, 1976; revision received May 5, 1976. This work was sponsored by the Air Force Advanced Ballistic Reentry Systems Agency (ABRES) under contract number F04701-75-C-0161.

Index categories: Boundary Layers and Convective Heat Transfer—Turbulent; Supersonic and Hypersonic Flow; LV/M Aerodynamic Heating.

*Manager, Atmospheric Dynamics Department. Member AIAA.
†Lieutenant, U. S. Air Force.